JOURNAL OF VIROLOGY, Dec. 2003, p. 12552–12561 Vol. 77, No. 23
0022-538X/03/$08.00+0 DOI: 10.1128/JVI.77.23.12552–12561.2003

Bystander Killing during Avian Leukosis Virus Subgroup B Infection Requires TVB^{S3} Signaling

Felipe Diaz-Griffero, Steven A. Hoschander, and Jürgen Brojatsch*

Department of Microbiology and Immunology, Albert Einstein College of Medicine, Bronx, New York 10461

Received 23 January 2003/Accepted 2 September 2003

Cell killing by avian leukosis virus subgroup B (ALV-B) in cultures has been extensively studied, but the molecular basis of this process has not been established. Here we show that superinfection, which has been linked to cell killing by ALV-B, plays no crucial role in cell death induction. Instead, we show that signaling by the ALV-B receptor, TVB^{S3}, a member of the tumor necrosis factor receptor family, is essential for ALV-B-mediated cell death. TVB^{S3} activated caspase-dependent apoptosis during ALV-B infection. Strikingly, apoptosis induction occurred predominantly in uninfected cells, while ALV-B-infected cells were protected against cell death. This bystander killing phenomenon was reproduced in a virus-free system by cocultivating ALV-B Env-expressing cells with TVB^{S3}-expressing cells. Taken together, our results indicated that ALV-B-mediated apoptosis is triggered by ALV-B Env–TVB^{S3} interactions.

Several retroviruses kill target cells in cultures, a phenomenon called the cytopathic effect. The cytopathicity of these retroviruses correlates with their pathogenicity in vivo. For example, human immunodeficiency virus (HIV) (24, 30) and a feline leukemia virus (FeLV) strain (FeLV-FAIDS) (15) are highly cytopathic in T cells, and infection of their natural hosts leads to a severe depletion of T cells, causing immunodeficiency. FeLV subgroup C (FeLV-C) kills erythroid progenitor cells in cultures and induces fatal aplastic anemia in newborn cats (5, 34). Furthermore, cytopathic murine leukemia virus Cas-Br-E kills cultured mouse thymocytes (40) and induces a neurodegenerative disease in mice (29). Finally, infections by equine infectious anemia virus (26) and avian leukosis virus (ALV) subgroup B (ALV-B) (22) exhibit cytopathic effects in fetal donkey dermal cells and primary chicken embryo fibroblasts (CEFs), respectively. Both cytopathic retroviruses induce severe anemia in their respective hosts (18, 35). Therefore, a comprehensive understanding of the cytopathicity of these retroviruses in cultures will enhance insight into their ability to trigger specific diseases.

Cell killing by cytopathic retroviruses has been correlated with superinfection, that is, repeated rounds of reinfection of target cells, which results in the accumulation of unintegrated viral DNA (UVD). For example, superinfection has been associated with the cytopathicity of HIV type 1 (HIV-1) (36), spleen necrosis virus (23), equine infectious anemia virus (31, 33), FeLV-FAIDS (15), and ALV-B (38, 39). However, the contribution of superinfection to retroviral cell killing remains to be elucidated.

ALV has been used as a model system for retroviral cell killing and is divided into cytopathic (B, D, and F) and noncytopathic (A, C, E, G, H, and I) subgroups (10). Infection of target cells by cytopathic ALVs leads to substantial cell death during the acute phase of infection, which is followed by a noncytopathic chronic phase (38, 39). Mapping experiments have indicated that the envelope glycoprotein (Env) of cytopathic ALV-B is essential for cell killing as well as receptor specificity (16). In addition, determinants for cell killing have been mapped to Env of different cytopathic retroviruses, including HIV-1 (8), avian hemangioma virus (32), murine leukemia virus Cas-Br-E (29), FeLV-C (34), and FeLV-FAIDS (15). These results suggested a critical role of viral Env-receptor interactions in retroviral cell killing. This suggestion is further supported by the fact that the receptor for cytopathic ALV-B, TVB^{S3}, contains three extracellular cysteine-rich domains, a single transmembrane region, and a putative cytoplasmic "death domain." Transient expression of TVB^{S3} in mammalian cells activates apoptosis, indicating that TVB^{S3} is a functional death receptor (6). TVB^{S3} is also able to activate an NF-κB-mediated antagonistic pathway that blocks apoptosis (9). Inhibition of this protective pathway by the protein biosynthesis inhibitor cycloheximide (CHX) or the I-κB "superrepressor" renders TVB^{S3}-expressing cells susceptible to killing by soluble ALV-B Env (9). However, the role of TVB^{S3} signaling in cell death induction during ALV-B infection remains to be determined.

In this study, we examined the contribution of TVB^{S3} signaling to cell killing during ALV-B infection. We showed that ALV-B infection activates TVB^{S3} signaling and caspase-dependent apoptosis. Strikingly, predominantly uninfected bystander cells were killed during ALV-B infection. This bystander killing phenomenon was reconstituted by cocultivation of ALV-B Env-expressing cells with TVB^{S3}-positive cells. Finally, massive UVD accumulation did not trigger cell death, indicating that ALV-B Env binding to TVB^{S3}, not superinfection, plays a crucial role in cell killing by ALV-B.

MATERIALS AND METHODS

Cell lines, plasmids, and viruses. QT6 quail cells and DF-1 CEFs were obtained from the American Type Culture Collection. Human 293-TVB^{S3} and QT6#24 cells were previously described (7, 14). 293 cells expressing either ALV-A Env or ALV-B Env (293-Env-A or 293-Env-B cells, respectively) were kindly provided by W. Mothes (28). Cells were grown in complete Dulbecco modified Eagle medium (Mediatech, Herndon, Va.) supplemented with 10%

* Corresponding author. Mailing address: Department of Microbiology and Immunology, Albert Einstein College of Medicine, Bronx, NY 10461. Phone: (718) 430-3079. Fax: (718) 430-8711. E-mail: brojatsc@aecom.yu.edu.

fetal bovine serum, 2 mM L-glutamine, 100 U of penicillin/ml, and 100 μg of streptomycin/ml. QT6 cells, seeded on 100-mm tissue culture plates, were transfected with 10 μg of pBK-TVB^{S3} or pBK-TVB^{S3}-F292A by using 20 μl of Lipofectamine (Gibco/BRL, Rockville, Md.). Single-cell clones were selected with 1 mg of G418 (Clontech, Palo Alto, Calif.)/ml and isolated by using cloning cylinders. Wild-type ALV-B was produced by transfecting DF-1 cells with ALV-A–green fluorescent protein (GFP) [pRCASBP(A)-eGFP] or ALV-B–GFP [pRCASBP(B)-eGFP] (28). Supernatants were collected 48 h after transfection and stored at −80°C. Viral titers were determined by using endpoint dilutions in DF-1 cells. GFP-positive cells were monitored after 6 to 10 days, and the viral titers were reported as infectious units per milliliter. Phosphate-buffered saline (PBS) was obtained from Cellgro.

Assay of cell killing by flow cytometry. A total of 10^5 DF-1 or QT6 cells expressing wild-type TVB^{S3} or signaling-deficient TVB^{S3}-F292A receptors were plated per well in a 24-well dish. Cells were infected with ALV-A–GFP or ALV-B–GFP at different multiplicities of infection (MOIs). Five days postinfection, cells were washed with PBS, trypsinized, and replated for 6 h. Cells were washed with PBS and trypsinized, and cell counts were determined by flow cytometry (FACSCalibur flow cytometer; Becton Dickinson Immunocytometry Systems) of propidium iodine-negative cells (Roche, Indianapolis, Ind.) with time as a fixed parameter.

Survival curve. A total of 10^5 DF-1 cells were infected with ALV-A–GFP or ALV-B–GFP at an MOI of 1. At each time point, cells were washed with PBS, trypsinized, and replated for 6 h, and surviving cells were counted.

Cell killing by soluble IgG (SU-IgG) proteins. A total of 10^5 DF-1 cells were plated per well in a 24-well dish and incubated for 4 days at 37°C. Subsequently, the cells were treated with 50 ng of soluble ALV-A and ALV-B Env fusion proteins (SUA-immunoglobulin G [IgG] and SUB-IgG) for 2 days. The numbers of surviving cells were determined by flow cytometry (see above). Cells were also processed for in situ cell death detection (see below).

Detection of apoptotic cells and infected cells by flow cytometry. A total of 10^5 DF-1 cells in a 24-well plate were infected with ALV-B for 5 days. Cells were harvested in Ca^{2+}- and Mg^{2+}-free PBS containing 1 mM EDTA and analyzed by flow cytometry as described above (41). Samples were analyzed in the FL-1 channel for the detection of GFP-positive cells and in the FL-4 channel for the detection of apoptotic cells by using an annexin V-Alexa 568 kit (Roche) according to the manufacturer's directions.

Flow cytometry for TVB- and GFP-positive cells. A total of 10^5 DF-1 cells in a 24-well plate were infected for 5 days, trypsinized, and replated to ensure the analysis of surviving cells. After 6 h, the cells were harvested in Ca^{2+}- and Mg^{2+}-free PBS containing 1 mM EDTA and prepared for flow cytometry as described previously (41). Briefly, 10^5 cells were incubated in 1 ml of medium containing SUB-IgG for 1 h. Subsequently, the cells were incubated with an anti-rabbit Cy5-labeled secondary antibody for 1 h. Samples were then analyzed with a FACSCalibur flow cytometer in the FL-1 channel to detect infected cells (GFP-positive cells) and in the FL-4 channel to detect receptor accessibility (Cy5-positive cells).

Fluorescence microscopy. Wide-field fluorescence microscopy was performed by using an Olympus IX70 microscope with filters for the red and green channels. Pictures were taken by using ×20 N.A. 0.4 phase 1 and ×40 LWD phase 2 lenses. Pictures were processed and mounted by using Photoshop software (Adobe Systems, San Jose, Calif.).

Southern blot analysis. Total genomic DNA was isolated from 2×10^6 infected DF-1 cells by using a genomic tip system (Qiagen, Valencia, Calif.). Undigested genomic DNA was concentrated by ethanol precipitation, quantitated and separated on 1% agarose gels, and transferred to nylon membranes. Southern analysis was performed by established procedures (27). A 1.5-kb *Sac*I/*Sac*II fragment derived from the Gag region of plasmid pRCASBP(A)-eGFP was ^{32}P labeled with a random-primed DNA labeling kit (Amersham Pharmacia, Piscataway, N.J.) and used as a probe to detect viral DNA. Hybridization was performed at 48°C with Ultrahyb buffer (Ambion, Austin, Tex.). The membranes were washed at 48°C with 2× SSC (1× SSC is 0.15 M NaCl plus 0.015 M sodium citrate)–0.1% sodium dodecyl sulfate and exposed to XAR-5 film (Kodak, Rochester, N.Y.) at −80°C.

Immunoblotting. Cell lines were grown on 100-mm tissue culture plates to a confluence of 90%. Extracts were prepared with homogenization buffer (10 mM Tris [pH 7.5], 10 mM NaCl, 1 mM EDTA) containing a cocktail of protease inhibitors (Roche). Cells were subjected to Dounce homogenization and centrifuged at 2,500 × *g* to obtain postnuclear supernatants. Protein concentrations were determined by using a bicinchoninic acid protein assay reagent kit (Pierce, Rockford, Ill.). Ten micrograms of protein was applied to 10% polyacrylamide–sodium dodecyl sulfate gels under reducing conditions and transferred to nitrocellulose membranes. The membranes were probed with SUB-recombinant IgG (7) to detect TVB^{S3} and then incubated with horseradish peroxidase-conjugated anti-rabbit immunoglobulin (Amersham Pharmacia). The TVB^{S3} signal was detected by using an enhanced chemiluminescence kit (Amersham Pharmacia).

In situ cell death detection (terminal deoxynucleotidyltransferase-mediated dUTP-biotin nick end labeling [TUNEL] assay). A total of 10^5 DF-1 cells were plated per well in a 24-well dish and infected with ALV-A–GFP or ALV-B–GFP at different MOIs. At 4, 5, and 6 days after infection, samples were fixed with 3.9% paraformaldehyde (Sigma, St. Louis, Mo.) in PBS (Mediatech) for 30 min. Detection of DNA strand breaks was performed by using an in situ cell death detection kit (TMR red; Roche) according to the manufacturer's directions. In brief, DNA breaks were detected by using terminal deoxynucleotidyltransferase and rhodamine-labeled dUTP.

Caspase 3 colorimetric assay. A total of 10^5 DF-1 cells were infected in 24-well plates with ALV-A and ALV-B at different MOIs. Protein extracts were prepared from infected cells on day 5 postinfection. Caspase 3 activity in cellular extracts was measured by using a caspase 3 colorimetric kit (R&D Systems, Inc., Minneapolis, Minn.) according to the manufacturer's directions.

RESULTS

Role of superinfection in ALV-B-mediated cell killing. Weller and coworkers correlated cytopathic effects during ALV-B infection with the accumulation of unintegrated viral DNA (UVD), presumably caused by superinfection (38, 39). In order to test whether cell killing by ALV-B is linked to superinfection, we tested UVD accumulation and cell death induction in cultures infected at increasing virus-to-cell ratios (MOIs).

To analyze cell killing by ALV-B, we established modified plaque-forming assays. cytopathic effects triggered by ALV-B have been studied traditionally with plaque-forming assays (16). In these assays, ALV-infected cells were overlaid with agar, and plaques were visualized with neutral red (16). We modified these plaque-forming assays by omitting the addition of top agar to infected cells; this modification allowed the quantification and molecular analysis of cell killing during ALV-B infection. The kinetics of cell killing and plaque formation following ALV-B infection of target cells were identical in the presence or absence of top agar (data not shown). The plaque-forming assays were performed with a CEF cell line, DF-1, which expresses endogenous TVB^{S3} as well as the ALV-A receptor TVA (2, 22).

To analyze the correlation between superinfection and cell killing, we challenged DF-1 cells at different MOIs and measured surviving cells 5 days postinfection by flow cytometry (Fig. 1A). Cytopathic effects following ALV-B infection were MOI dependent. The number of surviving cells decreased with the MOI of the incoming virus, and the lowest cell numbers were observed at an MOI of 1 (Fig. 1A). The decrease in the cell number on day 5 was concomitant with massive plaque formation, suggesting cell death induction by ALV-B. Surprisingly, the cell number increased again after ALV-B challenge at an MOI of 10 (Fig. 1A), indicating that ALV-B at high MOIs was not cytopathic. To analyze the inhibition of cell killing at higher MOIs (Fig. 1A), we challenged DF-1 cells at MOIs of 5, 10, and 50. ALV-B-mediated cell killing was completely inhibited at MOIs above 10 (Fig. 1B). As expected, cell killing was not detected in cells infected by ALV-A, regardless of the MOI tested (Fig. 1A). In addition, we challenged primary CEFs with ALV-A and ALV-B at increasing MOIs. As expected, CEFs showed cytopathic effects following ALV-B infection in an MOI-dependent fashion (Fig. 1C). In contrast, CEFs infected by ALV-A did not show cytopathic effects (Fig. 1C).

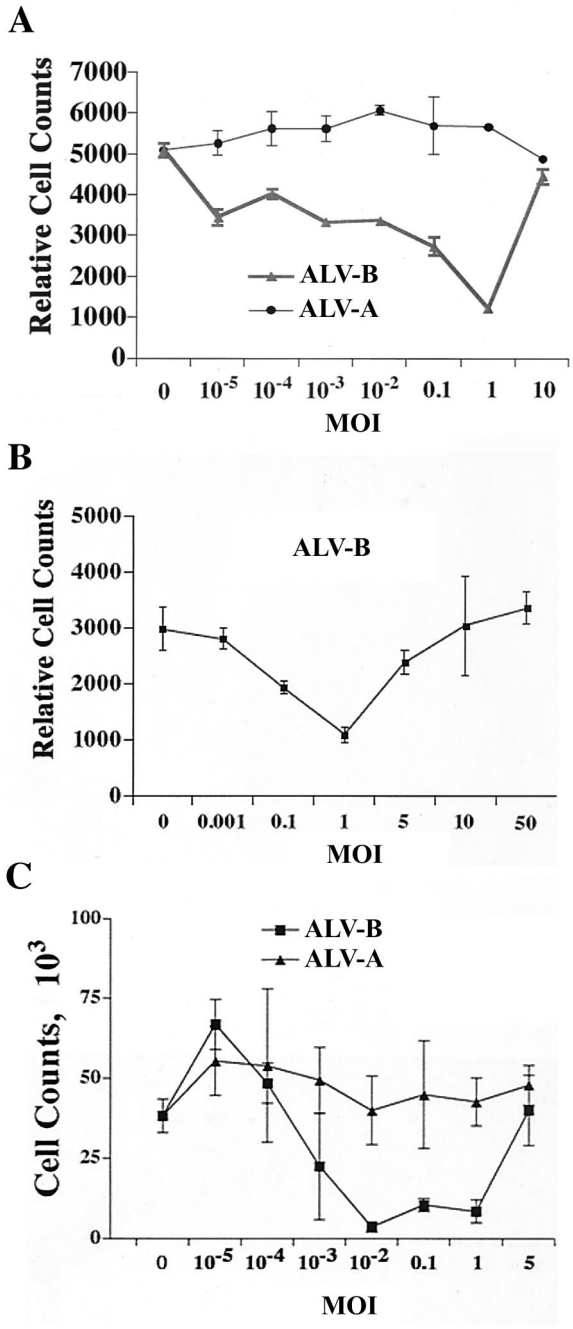

FIG. 1. ALV-B infection of target cells at high MOIs prevents cytopathic effects. (A) DF-1 cells were infected with ALV-A and ALV-B at different MOIs. Cells were replated and counted by flow cytometry 5 days postinfection. (B) DF-1 cells were infected with ALV-B at increasing MOIs. Surviving cells were replated and counted by flow cytometry 5 days postinfection. (C) Primary CEFs were infected with ALV-A and ALV-B at increasing MOIs and analyzed as described in Materials and Methods (survival curves). Experiments were performed in triplicate, and standard deviations are indicated.

To determine the correlation between superinfection and cytopathic effects during ALV-B infection, we challenged DF-1 cells with ALVs at increasing MOIs (0.1, 1, and 10) and measured UVD levels. UVD was isolated from adherent cells and

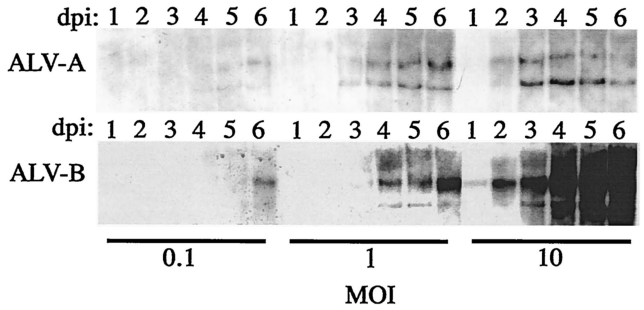

FIG. 2. ALV-B infection of target cells at high MOIs leads to the accumulation of unintegrated viral DNA. DF-1 cells were challenged with ALV-A and ALV-B at different MOIs, and total genomic DNA was isolated on a daily basis for a period of 6 days (dpi, days postinfection). Levels of unintegrated viral DNA were determined by Southern blot analysis with a radioactively labeled DNA fragment specific for the ALV Gag gene.

analyzed by Southern blotting with a radioactive ALV Gag DNA fragment as a probe (Fig. 2). As expected, UVD levels increased over time, and the strongest UVD signals were obtained 6 days postinfection (Fig. 2). In agreement with the findings of other groups, UVD levels were significantly higher in ALV-B-infected cells than in ALV-A infected cells, regardless of the MOI used. UVD levels increased with the MOI, and the highest UVD accumulation was detected at the highest MOI. Although ALV-B at an MOI of 10 led to the highest accumulation of UVD, infection at this high MOI did not trigger cell death. This result indicated that massive UVD accumulation was not toxic to cells (Fig. 2) and that a negative correlation existed between UVD levels and cell killing upon ALV-B challenge at a high MOI. In addition, maximal cell killing by ALV-B was observed at an MOI of 1, which led to significantly less UVD accumulation than ALV-B at an MOI of 10. These UVD levels were only slightly higher than those observed in ALV-A-infected cells. Taken together, our results showed that cell killing by ALV-B cannot be explained by the accumulation of UVD.

TVB^{S3} signaling is required for ALV-B-mediated cell killing. Since high UVD levels were not toxic to cells, we assessed whether ALV-B-induced cell killing is mediated by signaling by the ALV-B receptor, TVB^{S3} (6, 7, 16). To test the involvement of the death receptor TVB^{S3} in ALV-B-mediated cell killing, we expressed wild-type or signaling-deficient TVB^{S3} in QT6 cells, which lack endogenous TVB^{S3}. Signaling-deficient TVB^{S3} contains a substitution of a highly conserved residue in the cytoplasmic death domain (TVB^{S3}-F292A). Mutation of this residue inhibits signaling by TVB^{S3} (6, 9), while it has no effect on ALV-B entry. Receptor expression levels were high in cell clones QT6-TVB^{S3}#24, QT6-TVB^{S3}-FA211, and QT6-TVB^{S3}-FA212 and low in QT6-TVB^{S3}-4 (Fig. 3A), as determined by Western blotting. To confirm that the expressed receptors are signaling competent, QT6-TVB^{S3} and QT6-TVB^{S3}-F292A cells were incubated with SU-IgG and the protein biosynthesis inhibitor CHX. ALV Env fusion proteins are comprised of the soluble part of ALV Env fused in frame with the constant region of an immunoglobulin heavy chain (7). As predicted, QT6-TVB^{S3} cells were killed in the presence of SUB-IgG and CHX, while no killing was observed for QT6-

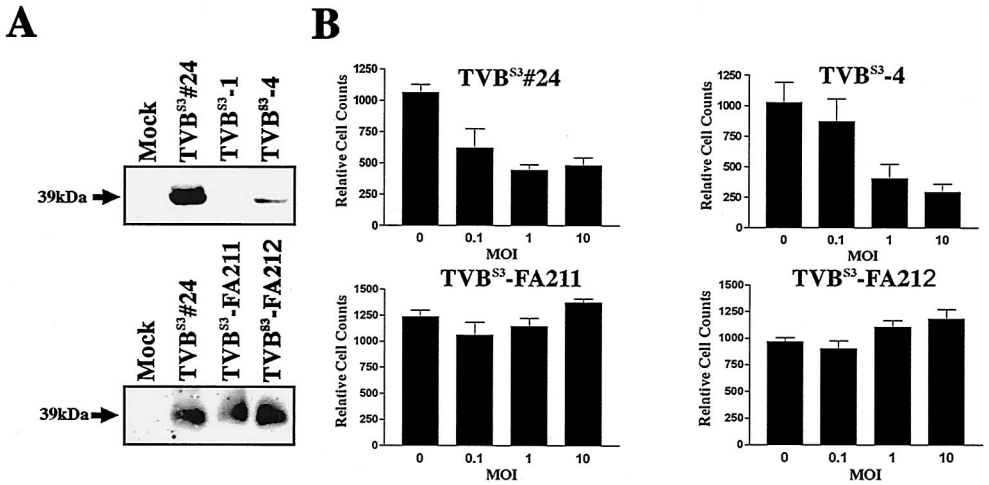

FIG. 3. TVB^{S3} signaling is essential for ALV-B-mediated cell killing. (A) Western blot analysis of protein extracts derived from QT6 cells expressing either wild-type TVB^{S3} (TVB^{S3}#24, TVB^{S3}-1, and TVB^{S3}-4) or mutant TVB^{S3}-F292A (TVB^{S3}-FA211 and TVB^{S3}-FA212) was performed with SUB-IgG to detect TVB^{S3} expression. Western blot analysis identified a 39-kDa band for TVB^{S3} and TVB^{S3}-F292A. (B) QT6 cells expressing either wild-type TVB^{S3} (TVB^{S3}#24 and TVB^{S3}-4) or mutant TVB^{S3}-F292A (TVB^{S3}-FA211 and TVB^{S3}-FA212) were infected with ALV-B at different MOIs. Cells were replated, and cell counts were determined by flow cytometry 5 days postinfection. Experiments were performed in triplicate, and standard deviations are indicated.

TVB^{S3}-F292A cells (data not shown). Furthermore, no cell death was induced by SUA-IgG, which was derived from noncytopathic ALV-A. These results confirmed that wild-type TVB^{S3} expressed in QT6 cells is signaling competent.

To determine whether TVB^{S3} signaling is required for ALV-B-induced cell killing, we challenged QT6-TVB^{S3} or QT6-TVB^{S3}-F292A cells with ALV-B at different MOIs and measured surviving cells by flow cytometry at day 5 postinfection. QT6-TVB^{S3} and QT6-TVB^{S3}-F292A cells did not differ in their susceptibilities to ALV-B infection and viral spread, as measured by flow cytometry with ALV-B–GFP (data not shown). As predicted, QT6-TVB^{S3} cells but not QT6-TVB^{S3}-F292A cells were killed upon ALV-B infection (Fig. 3B). Killing of QT6-TVB^{S3} cells was MOI dependent, and maximal cell killing was observed at an MOI of 10 (Fig. 3B). Viral spread was slower in QT6 cells than in DF-1 cells, thereby allowing killing at the higher MOI (i.e., 10). These results suggested that signaling by TVB^{S3} is essential for cell killing by ALV-B. Involvement of the death receptor TVB^{S3} in ALV-B-mediated cytopathic effects implied killing by apoptosis during ALV-B infection.

ALV-B infection triggers apoptosis. TVB^{S3}, a member of the tumor necrosis receptor family, triggers apoptosis pathways upon activation in mammalian cells (6, 9). To study apoptosis induction during ALV-B infection, we challenged DF-1 cells with noncytopathic ALV-A (ALV-A–GFP) and cytopathic ALV-B (ALV-B–GFP) at an MOI of 1. Cytopathic effects were measured by counting surviving cells over a period of 10 days postinfection. The survival curves for ALV-A- and ALV-B-infected DF-1 cells were identical during the first 4 days of infection (Fig. 4A). This initial noncytopathic period of ALV-B infection was followed by massive cell death induction and plaque formation 5 days postinfection; maximal cell killing (60%) occurred 7 days postinfection (Fig. 4A). Following the acute phase of infection, cells entered the chronic phase, in which cytopathic effects were not observed and cells resumed proliferation (Fig. 4A).

We hypothesized that ALV-B infection triggers apoptosis via TVB^{S3} signaling. Apoptosis induction was measured by TUNEL and caspase 3 cleavage assays. The TUNEL assay identifies low-molecular-weight DNA in cells undergoing apoptosis. DF-1 cells infected with ALV-B at an MOI of 1 were assayed for apoptosis induction 4, 5, and 6 days postinfection (Fig. 4B). Apoptosis was not observed 4 days postinfection, consistent with cell-killing measurements (Fig. 4A). However, substantial apoptosis induction and plaque formation occurred in ALV-B-infected DF-1 cells at days 5 and 6 postinfection (Fig. 4B). Apoptotic cells accumulated in the periphery of plaques, while the central portion of the plaques was nearly devoid of cells, presumably as a result of massive cell killing (Fig. 4B).

Mammalian death receptors trigger apoptosis by activating cellular caspases (1, 19). To test caspase involvement in ALV-B-mediated apoptosis, we used a colorimetric assay to detect caspase 3 activity. Protein extracts from DF-1 cells challenged with ALV-A and ALV-B at different MOIs were assayed for caspase 3 activity 5 days postinfection (Fig. 4C). Caspase 3 activity was markedly enhanced in ALV-B-infected cultures at increasing MOIs, and the highest activity was observed at an MOI of 1 (Fig. 4C). The caspase 3 activity obtained at an MOI of 1 was comparable to the activity measured in DF-1 cells treated with the apoptosis inducer staurosporine (Fig. 4C). Caspase 3 activity was not observed at an MOI of 10, consistent with the fact that ALV-B at a high MOI does not kill DF-1 cells (Fig. 1B). As expected, caspase 3 activation was not observed in ALV-A-infected cells (Fig. 4C). The caspase 3 activation occurred simultaneous with the reduction in the number of surviving cells and plaque formation on day 5 (Fig. 4A).

To support the hypothesis that caspases are involved in ALV-B-mediated cell killing, we used the caspase inhibitor

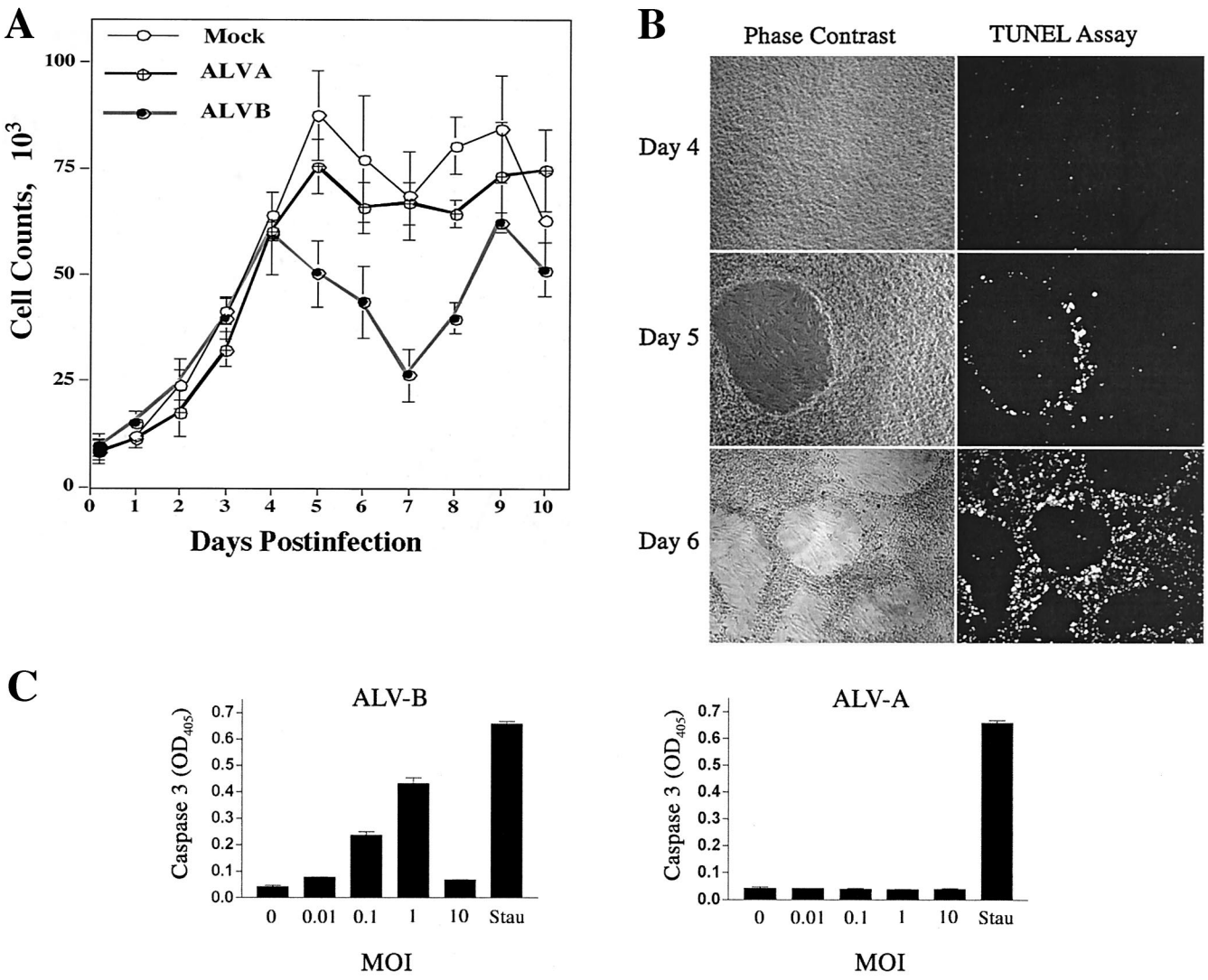

FIG. 4. Activation of apoptosis by ALV-B infection of target cells. (A) DF-1 cells were infected with ALV-A and ALV-B at an MOI of 1, and surviving cells were determined after replating on a daily basis for a period of 10 days as described in Materials and Methods (survival curve). (B) Apoptosis induction by ALV-B. DF-1 cells were challenged with ALV-B at an MOI of 1. Phase-contrast imaging and TUNEL staining were performed 4, 5, and 6 days postinfection. (C) Activation of caspase 3 upon ALV-B infection of DF-1 cells. DF-1 cells were challenged with ALV-A and ALV-B at different MOIs, and caspase 3 activity in cellular extracts was analyzed by using a colorimetric assay 5 days postinfection. OD_{405}, optical density at 405 nm. The apoptosis inducer staurosporine was used as a positive control (1 μM for 3 h [Stau]). (D) DF-1 cells were challenged with ALV-B at different MOIs and treated with 20 μM zVAD-fmk (caspase inhibitor VI) 4 days postinfection. Cells were replated and counted 5 days postinfection. Experiments were performed in triplicate, and standard deviations are indicated.

zVAD-fmk (Calbiochem, La Jolla, Calif.) (6, 25). DF-1 cells infected with ALV-B at different MOIs were treated with 20 mM zVAD-fmk 4 days postinfection, and surviving cells were measured by flow cytometry 6 days postinfection. This caspase inhibitor reduced ALV-B-mediated cell killing from 70 to 30% at an MOI of 0.1, supporting the hypothesis that cell killing is caspase dependent (Fig. 4D). zVAD-fmk treatment also inhibited plaque formation, indicating that apoptosis induction is required for plaque formation. Taken together, these results suggested that the reduction in the number of surviving cells during the acute phase of ALV-B infection is caused by caspase-mediated apoptosis via TVB^{S3} signaling.

Bystander killing by ALV-B. To monitor viral spread during cell death progression, we used ALV-B–GFP (14). Cells infected with ALV-B–GFP were distinguished from uninfected cells by GFP expression. DF-1 cells infected at an MOI of 1 were analyzed for apoptosis induction by TUNEL staining on day 5 postinfection. We found that apoptotic (Fig. 5B) and infected (Fig. 5C) cells accumulated in the periphery of plaques (Fig. 5A). Surprisingly, the apoptotic and infected cell populations were not identical (Fig. 5D). In fact, the majority of apoptotic cells (>95%) were GFP negative (Fig. 5D). These results indicated bystander killing of GFP-negative, presumably uninfected cells during ALV-B infection. Furthermore, only a few infected cells (GFP positive) were apoptotic, suggesting that infected cells were protected against cell killing.

To support the hypothesis of bystander killing during ALV-B infection, we challenged DF-1 cells with ALV-B and

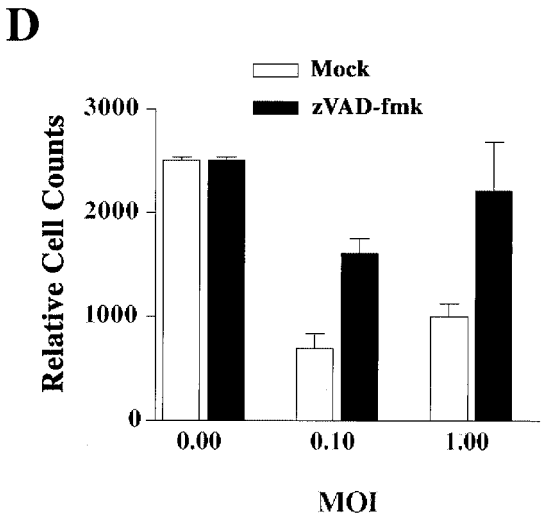

FIG. 4—*Continued.*

analyzed viral spread by GFP expression and apoptosis induction by annexin V binding. Increased cell surface annexin V binding is caused by a loss of asymmetry in cell membrane phospholipids during apoptosis induction (37). DF-1 cells infected with ALV-B–GFP at an MOI of 1 were analyzed for GFP expression and annexin V binding by flow cytometry 5 days postinfection (Fig. 5E and F). A significant increase in the number of annexin V-positive cells was detected in ALV-B-infected DF-1 cells. Consistent with previous observations, the majority of the apoptotic cells were uninfected (GFP negative); only a fraction of the apoptotic cells was infected (Fig. 5F).

ALV-B Env-mediated cell killing. To test whether the killing of uninfected bystander cells was triggered by viral Env-TVB^{S3} interactions during ALV-B infection, we treated DF-1 cells with SU-IgG at different time points postplating (days 1 and 4) and determined cell killing 2 days after SU-IgG treatment. Surviving cells were measured by flow cytometry, and apoptotic cells were measured by TUNEL assays (Fig. 6A and B). Massive cell killing (Fig. 6A) and apoptosis induction (Fig. 6B) were observed in DF-1 cells treated with SUB-IgG 4 days postplating. In contrast, cell killing was not observed in DF-1 cells treated with SUB-IgG 1 day postplating. As expected, cell death induction was not detected with SUA-IgG, which was derived from noncytopathic ALV-A, regardless of the time point of SUA-IgG administration (Fig. 6A and B). These results showed that SUB-IgG–receptor interactions reproduce cell killing in a virus-free system 4 days postplating.

To determine whether the native ALV-B envelope glycoprotein expressed on the cellular surface kills uninfected cells, we performed cocultivation experiments. Human 293-Env-A or 293-Env-B cells (28) were cocultivated with DF-1 cells at a 1:40 ratio. Massive cell killing and plaque formation were observed in cocultivation experiments with 293-Env-B cells on day 5 postplating, while cell killing was not detected with 293-Env-A cells (Fig. 6C). This experiment represented the major cytopathic effects during ALV-B infection, such as apoptosis induction and plaque formation (Fig. 6C). Therefore, the bystander killing phenomenon could be explained by interactions between ALV-B Env-expressing infected cells and TVB^{S3}-expressing uninfected cells. Taken together, these results suggested that cell killing during ALV-B infection is mediated by ALV-B Env–TVB^{S3} interactions.

Cell surface accessibility of TVB^{S3} and cell killing by ALV-B. DF-1 cells infected with ALV-B were resistant to cell killing (Fig. 5). We hypothesized that ALV-B infection leads to ALV-B Env expression and a subsequent reduction in TVB^{S3} cell surface accessibility, which might protect infected cells from cytopathic effects. In order to measure TVB^{S3} cell surface accessibility in response to ALV-B Env expression, we transfected 293-TVB^{S3} cells with increasing amounts of ALV-B Env expression constructs. TVB^{S3} cell surface accessibility was determined by flow cytometry with SUB-IgG. TVB^{S3} was not accessible on the surface of ALV-B Env-transfected cells, suggesting downregulation from the cell surface, presumably caused by ALV-B Env–receptor interactions (data not shown).

To test whether TVB^{S3} cell surface accessibility decreases during ALV-B–GFP infection, we measured receptor surface accessibility and GFP expression (viral spread) by flow cytometry. DF-1 cells infected with ALV-B–GFP at different MOIs were replated 5 days postinfection to analyze surviving cells. Subsequently, cells were tested for TVB^{S3} cell surface accessibility with SUB-IgG, and infection status was scored by analyzing GFP expression (Fig. 7). The number of infected cells increased with the MOI, while the amount of available TVB^{S3} decreased. At the highest MOI (i.e., 100), 98.5% of cells were GFP positive and TVB^{S3} negative. These results indicated that ALV-B infection reduces the amount of free TVB^{S3} receptors on the surface of infected cells.

Strikingly, after ALV-B challenge at an MOI of 1, a significant fraction of GFP-negative cells (27.5%) had low TVB^{S3} cell surface expression levels (Fig. 7). Reduced TVB^{S3} levels on these GFP-negative cells suggested that these cells were actually infected. These cells were presumably infected at a later time point, and GFP expression was below the threshold of detection. This notion is consistent with the facts that GFP expression was delayed and was detected only about 48 h after ALV-B challenge of DF-1 cells (data not shown). Our experiments showed that 93.5% of surviving DF-1 cells challenged with ALV-B at an MOI of 1 were TVB^{S3} negative and presumably infected. However, only a fraction of these cells was GFP positive, indicating that the GFP data underestimate the actual number of infected cells. In addition, predominantly GFP-negative cells were killed during ALV-B infection (Fig. 5), and it is possible that some of these cells were actually infected but expressed TVB^{S3} cell surface levels sufficient to trigger cell death.

The decrease in TVB^{S3} cell surface accessibility was not caused by changes in the total cellular levels of TVB^{S3}, as measured by Western blot analysis (data not shown). Taken together, our results suggested that highly infected cells are protected against cell killing by ALV-B as a result of reduced TVB^{S3} cell surface accessibility, indicating that TVB^{S3} cell surface expression is essential for cell killing.

DISCUSSION

Role of TVB in cell killing. Cell killing by ALV-B has been linked to the receptor binding region of ALV-B Env (16),

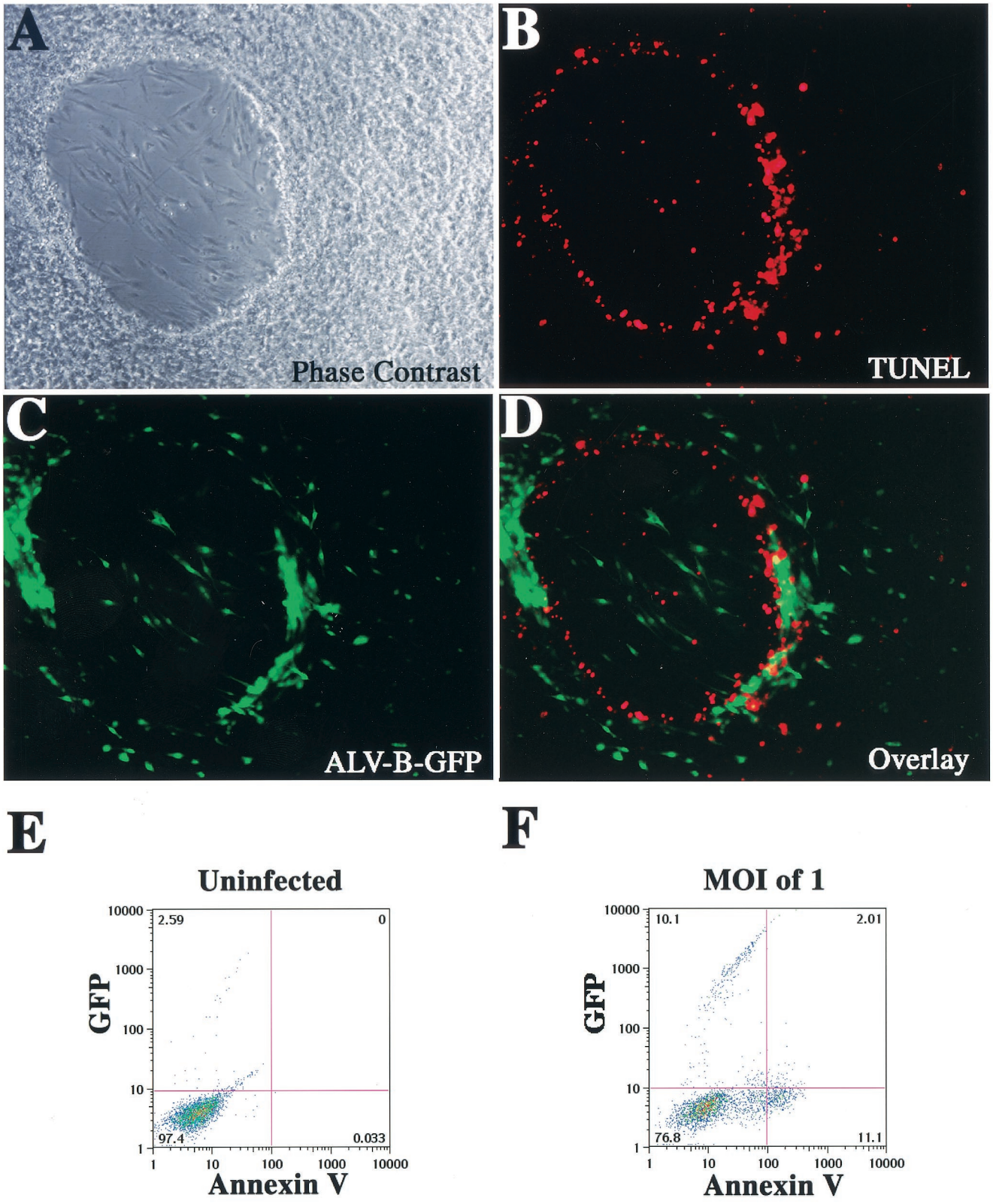

FIG. 5. Bystander killing of DF-1 cells during ALV-B infection. (A) DF-1 cells were infected at an MOI of 1 and fixed in paraformaldehyde 5 days postinfection. Plaque formation is shown by phase-contrast imaging. (B) Fixed DF-1 cells were subjected to TUNEL staining 5 days postinfection; apoptotic cells are shown in red. (C) Cells infected with ALV-B–GFP are shown in green. (D) Overlay of infected (green) and apoptotic (red) cells. (E and F) DF-1 cells were infected at an MOI of 1 and analyzed for annexin V binding 5 days postinfection. Infected (GFP-positive) cells and apoptotic (annexin V-positive) cells were quantitated by flow cytometry.

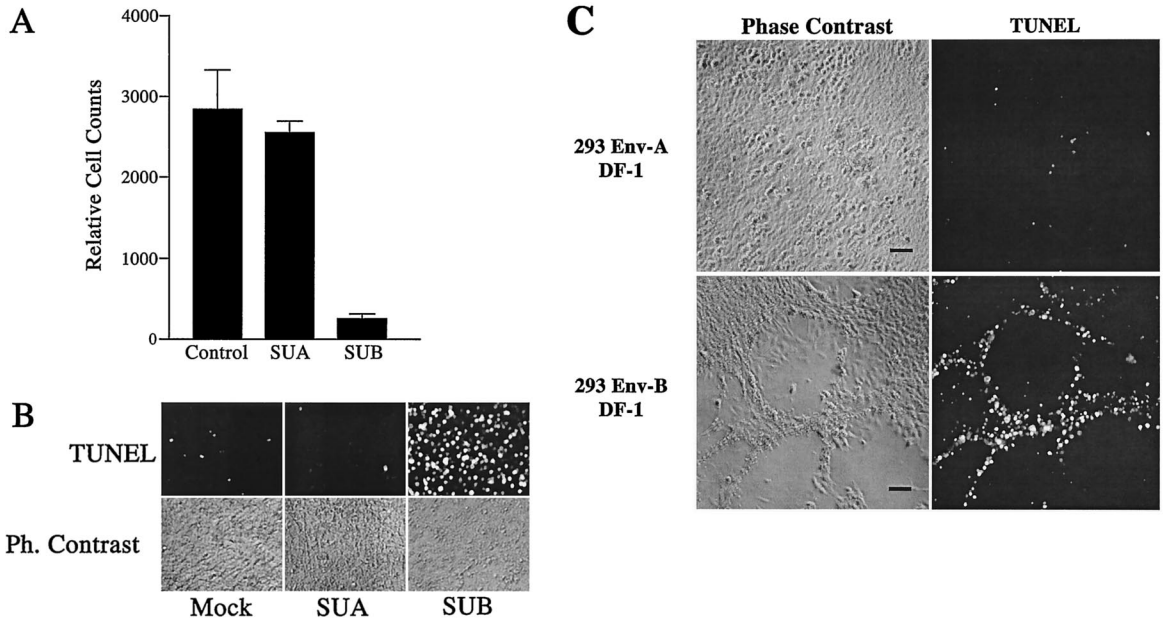

FIG. 6. ALV-B Env–receptor interactions activate apoptosis in DF-1 cells. (A) DF-1 cells were incubated with SUA-IgG and SUB-IgG 4 days postplating. Cells were replated and counted by flow cytometry 6 days postplating. Experiments were performed in triplicate, and standard deviations are indicated. (B) DF-1 cells were treated as described for panel A, fixed in paraformaldehyde and subjected to TUNEL staining 6 days postplating. Ph., phase. (C) DF-1 cells and 293-Env-A or 293-Env-B cells were cocultivated at a 40:1 ratio. Cells were fixed in paraformaldehyde and subjected to TUNEL staining 5 days postcocultivation. Phase-contrast images and TUNEL staining are shown. Bars, 10 μm.

suggesting involvement of the ALV-B receptor in this process. This suggestion is further supported by the fact that the ALV-B receptor TVB^{S3} belongs to the TNFR family (7) and is able to activate apoptosis (6, 7). In this work, we presented several findings that directly link TVB^{S3} signaling to cell killing by ALV-B. (i) The cytoplasmic death domain of TVB^{S3} was essential for cell killing by ALV-B. A single point mutation in the cytoplasmic tail of TVB^{S3} prevented receptor signaling and ALV-B-induced cell killing, while it did not interfere with ALV-B entry. (ii) ALV-B infection triggered apoptosis in a caspase-dependent fashion, presumably by direct activation of TVB^{S3}. (iii) Binding of soluble ALV-B Env to TVB^{S3} activated apoptosis. (iv) Cytopathic effects and plaque formation could be reconstituted by cocultivation of ALV-B Env-expressing cells with TVB^{S3}-expressing cells. (v) Uninfected cells were major targets for cell killing during ALV-B infection. Bystander killing was apparently caused by interactions of ALV-B Env expressed on the surface of infected cells with TVB^{S3} expressed on uninfected or minimally infected cells. (vi) TVB^{S3} cell surface accessibility was required for cell killing by ALV-B. ALV-B infection reduced the amount of free TVB^{S3} on the surface of infected cells and might protect these cells from cytopathic effects. Taken together, these results strongly suggested that the reduction in cell numbers following ALV-B infection is triggered by TVB^{S3}-mediated apoptosis and not by cell growth retardation.

ALV-B shares with reovirus serotypes 1 and 3 the ability to activate death receptor-mediated apoptosis. However, ALV-B is the only cytopathic retrovirus known to use a death receptor to enter target cells. The cell-killing mechanism of most cytopathic retroviruses remains to be determined, and it is possible that other cytopathic retroviruses also interact with death proteins and activate apoptotic pathways.

Initial and acute phases of ALV-B infection. ALV-B Env–TVB^{S3} interactions appear to be essential for cell killing by ALV-B. However, these interactions trigger cell death only under specific conditions, and cell killing is not observed during early rounds of ALV-B infection. Chi et al. previously showed that ALV-B infection of TVB^{S3}-positive cells activates an NF-κB-mediated protective pathway (9). It is conceivable that the activation of this antiapoptotic pathway keeps cells alive during the early phase of ALV-B infection. Suppression of the protective pathway may occur at the onset of ALV-B-mediated cell killing. It remains to be determined whether and how this protective pathway is suppressed during the killing phase of ALV-B infection. It is possible that proapoptotic factors, such as Smac/Diablo, override antiapoptotic proteins during the acute phase of infection and promote cell death (17).

Signaling by TNFR is regulated by phosphorylation, and apoptosis induction is triggered only by the unphosphorylated state of the receptor (11, 12). It is conceivable that phosphorylation of the cytoplasmic tail of TVB^{S3} regulates apoptosis induction. It remains to be shown whether the signaling state of TVB^{S3} is switched by phosphorylation during ALV-B infection.

Bystander killing. We observed killing of uninfected or minimally infected bystander DF-1 cells during ALV-B infection. Uninfected or minimally infected cells killed during ALV-B infection were adjacent to infected cells, suggesting that by-

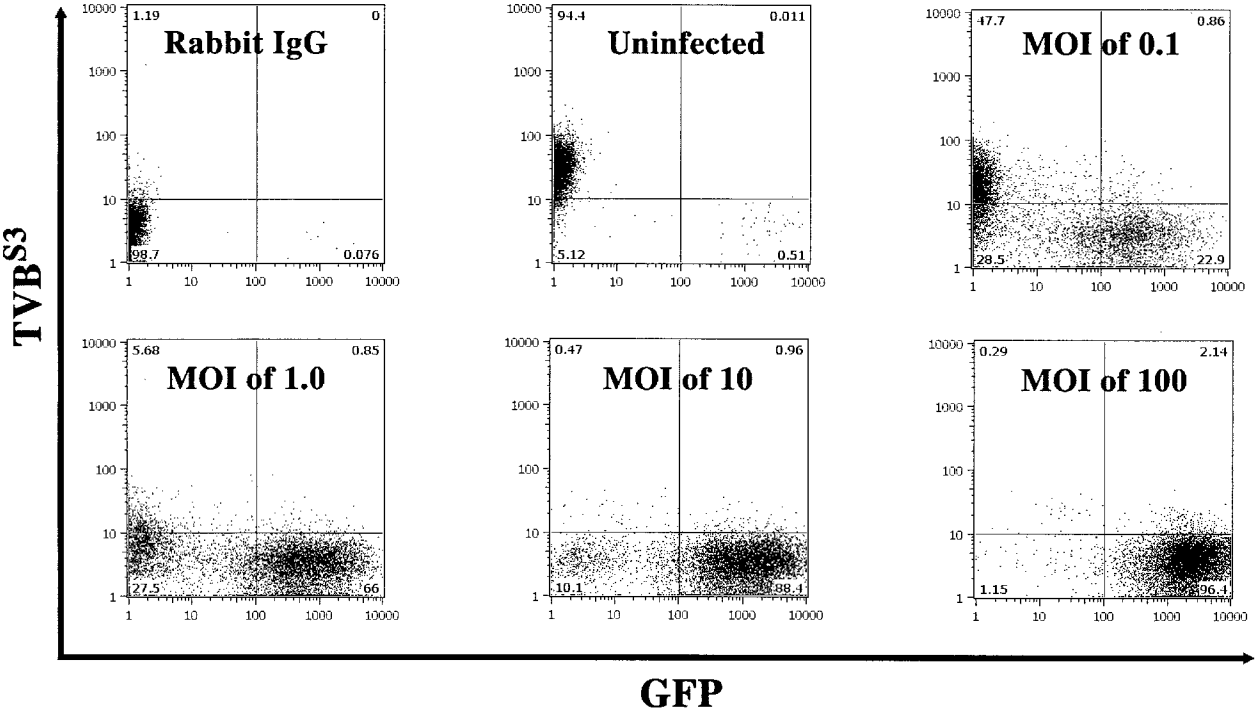

FIG. 7. Surface accessibility of TVB^{S3} in ALV-B-infected DF-1 cells. DF-1 cells were challenged with ALV-B at different MOIs for 5 days. Subsequently, cells were replated, resuspended, and incubated with SUB-IgG and anti-rabbit Cy5-labeled secondary antibody. Cells were analyzed for infection (GFP expression) and surface accessibility of TVB^{S3} (Cy5) by flow cytometry. An isotype-matched control was treated with rabbit IgG.

stander killing was triggered by interactions between ALV-B Env-expressing cells and TVB^{S3}-expressing cells (Fig. 8). This suggestion was supported by the fact that ALV-B Env-expressing cells and soluble ALV-B Env were able to kill TVB^{S3}-expressing avian cells. Retroviral spread requires that viral producer cells be alive. Therefore, killing of infected cells would be highly detrimental for viral spread, while bystander killing would not interfere with virus propagation by already infected cells. However, bystander killing would still diminish the number of potential target cells.

Bystander killing has also been postulated in the pathology of HIV. A massive loss of uninfected $CD8^+$ T cells has been observed in lymph nodes of HIV-1-infected patients. $CD8^+$-T-cell depletion can be reproduced in vitro by cocultivating HIV-1-infected $CD8^+$ T cells with macrophages (13, 21). HIV-1 infection of $CD8^+$ T cells does not trigger cytopathic effects in the absence of macrophages, suggesting that macrophage–$CD8^+$-T-cell interactions are essential for T-cell killing in cultures (20, 21). In addition, neurons are killed by soluble or membrane-bound HIV Env (3, 4), even though neurons are not susceptible to HIV infection. These results suggest that HIV Env binding to a specific neuronal receptor triggers cell death (3, 4).

Role of superinfection in ALV-B-mediated cell killing. Superinfection and accumulation of UVD have been correlated with cell killing by a series of cytopathic retroviruses, including ALV-B (15, 23, 31, 33, 36, 38, 39). In agreement with other groups, we found that UVD accumulation is significantly higher in cells infected by ALV-B than in cells infected by noncytopathic ALV-A. However, we found that the accumulation of UVD does not correlate with cell killing by ALV-B. In fact, we observed the highest accumulation of UVD in DF-1 cells infected with ALV-B at an MOI that did not promote cell killing. Therefore, UVD accumulation could be uncoupled from cell killing by ALV-B. Apparently, superinfection and UVD accumulation occur in infected cells which are actually protected against cell killing during ALV-B infection. The involvement of superinfection was further challenged by the bystander killing phenomenon, in which uninfected or minimally infected cells are killed during ALV-B infection. Taken together, our results showed that TVB^{S3} signaling, not superinfection, is essential for cell killing by ALV-B.

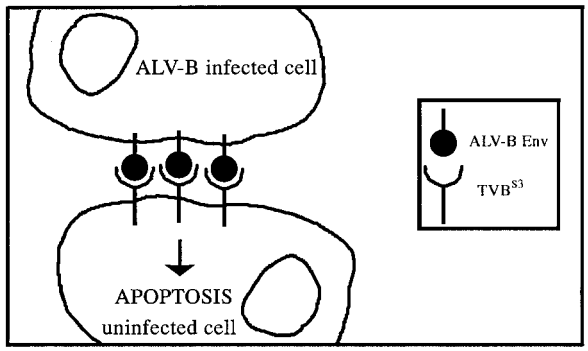

FIG. 8. Schematic representation of the bystander killing phenomenon during ALV-B infection of target cells. ALV-B Env expressed on infected cells interacts with TVB^{S3} expressed on uninfected cells and activates apoptotic pathways.

ACKNOWLEDGMENTS

We thank Elliott Schwarzenberger and Yuling Chi for helpful discussions and technical assistance. In addition, we thank Steve Porcelli, Scott Garforth, Volker Briken, Ken Samberg, and Yehoshua Levine for critical reading of the manuscript.

REFERENCES

1. **Ashkenazi, A., and V. M. Dixit.** 1998. Death receptors: signaling and modulation. Science **281:**1305–1308.
2. **Bates, P., J. A. Young, and H. E. Varmus.** 1993. A receptor for subgroup A Rous sarcoma virus is related to the low density lipoprotein receptor. Cell **74:**1043–1051.
3. **Brenneman, D. E., J. Hauser, C. Y. Spong, T. M. Phillips, C. B. Pert, and M. Ruff.** 1999. VIP and D-ala-peptide T-amide release chemokines which prevent HIV-1 GP120-induced neuronal death. Brain Res. **838:**27–36.
4. **Brenneman, D. E., G. L. Westbrook, S. P. Fitzgerald, D. L. Ennist, K. L. Elkins, M. R. Ruff, and C. B. Pert.** 1988. Neuronal cell killing by the envelope protein of HIV and its prevention by vasoactive intestinal peptide. Nature **335:**639–642.
5. **Brojatsch, J., B. S. Kristal, G. A. Viglianti, R. Khiroya, E. A. Hoover, and J. I. Mullins.** 1992. Feline leukemia virus subgroup C phenotype evolves through distinct alterations near the N terminus of the envelope surface glycoprotein. Proc. Natl. Acad. Sci. USA **89:**8457–8461.
6. **Brojatsch, J., J. Naughton, H. B. Adkins, and J. A. Young.** 2000. TVB receptors for cytopathic and noncytopathic subgroups of avian leukosis viruses are functional death receptors. J. Virol. **74:**11490–11494.
7. **Brojatsch, J., J. Naughton, M. M. Rolls, K. Zingler, and J. A. Young.** 1996. CAR1, a TNFR-related protein, is a cellular receptor for cytopathic avian leukosis-sarcoma viruses and mediates apoptosis. Cell **87:**845–855.
8. **Cheng-Mayer, C., T. Shioda, and J. A. Levy.** 1991. Host range, replicative, and cytopathic properties of human immunodeficiency virus type 1 are determined by very few amino acid changes in Tat and gp120. J. Virol. **65:** 6931–6941.
9. **Chi, Y., F. Diaz-Griffero, C. Wang, J. A. Young, and J. Brojatsch.** 2002. An NF-κB-dependent survival pathway protects against cell death induced by TVB receptors for avian leukosis viruses. J. Virol. **76:**5581–5587.
10. **Coffin, J. M., S. H. Hughes, and H. E. Varmus.** 1997. Retroviruses, p. 74. Cold Spring Harbor Labotaory Press, Cold Spring Harbor, N.Y.
11. **Cottin, V., A. Van Linden, and D. W. Riches.** 1999. Phosphorylation of tumor necrosis factor receptor CD120a (p55) by p42(mapk/erk2) induces changes in its subcellular localization. J. Biol. Chem. **274:**32975–32987.
12. **Cottin, V., A. A. Van Linden, and D. W. Riches.** 2001. Phosphorylation of the tumor necrosis factor receptor CD120a (p55) recruits Bcl-2 and protects against apoptosis. J. Biol. Chem. **276:**17252–17260.
13. **Davis, I. C., M. Girard, and P. N. Fultz.** 1998. Loss of $CD4^+$ T cells in human immunodeficiency virus type 1-infected chimpanzees is associated with increased lymphocyte apoptosis. J. Virol. **72:**4623–4632.
14. **Diaz-Griffero, F., S. A. Hoschander, and J. Brojatsch.** 2002. Endocytosis is a critical step in entry of subgroup B avian leukosis viruses. J. Virol. **76:**12866–12876.
15. **Donahue, P. R., S. L. Quackenbush, M. V. Gallo, C. M. deNoronha, J. Overbaugh, E. A. Hoover, and J. I. Mullins.** 1991. Viral genetic determinants of T-cell killing and immunodeficiency disease induction by the feline leukemia virus FeLV-FAIDS. J. Virol. **65:**4461–4469.
16. **Dorner, A. J., and J. M. Coffin.** 1986. Determinants for receptor interaction and cell killing on the avian retrovirus glycoprotein gp85. Cell **45:**365–374.
17. **Du, C., M. Fang, Y. Li, L. Li, and X. Wang.** 2000. Smac, a mitochondrial protein that promotes cytochrome c-dependent caspase activation by eliminating IAP inhibition. Cell **102:**33–42.
18. **Graf, T., B. Royer-Pokora, G. E. Schubert, and H. Beug.** 1976. Evidence for the multiple oncogenic potential of cloned leukemia virus: in vitro and in vitro studies with avian erythroblastosis virus. Virology **71:**423–433.
19. **Hengartner, M. O.** 2000. The biochemistry of apoptosis. Nature **407:**770–776.
20. **Herbein, G., U. Mahlknecht, F. Batliwalla, P. Gregersen, T. Pappas, J. Butler, W. A. O'Brien, and E. Verdin.** 1998. Apoptosis of CD8+ T cells is mediated by macrophages through interaction of HIV gp120 with chemokine receptor CXCR4. Nature **395:**189–194.
21. **Herbein, G., C. Van Lint, J. L. Lovett, and E. Verdin.** 1998. Distinct mechanisms trigger apoptosis in human immunodeficiency virus type 1-infected and in uninfected bystander T lymphocytes. J. Virol. **72:**660–670.
22. **Himly, M., D. N. Foster, I. Bottoli, J. S. Iacovoni, and P. K. Vogt.** 1998. The DF-1 chicken fibroblast cell line: transformation induced by diverse oncogenes and cell death resulting from infection by avian leukosis viruses. Virology **248:**295–304.
23. **Keshet, E., and H. M. Temin.** 1979. Cell killing by spleen necrosis virus is correlated with a transient accumulation of spleen necrosis virus DNA. J. Virol. **31:**376–388.
24. **Kowalski, M., J. Potz, L. Basiripour, T. Dorfman, W. C. Goh, E. Terwilliger, A. Dayton, C. Rosen, W. Haseltine, and J. Sodroski.** 1987. Functional regions of the envelope glycoprotein of human immunodeficiency virus type 1. Science **237:**1351–1355.
25. **Lin, Y., A. Devin, Y. Rodriguez, and Z. G. Liu.** 1999. Cleavage of the death domain kinase RIP by caspase-8 prompts TNF-induced apoptosis. Genes Dev. **13:**2514–2526.
26. **Madden, C. R., and D. S. Shih.** 1996. Analysis of the long terminal repeat from a cytopathic strain of equine infectious anemia virus. Virology **225:**395–399.
27. **Maniatis, T., E. F. Fritsch, and J. Sambrook.** 1982. Molecular cloning: a laboratory manual, p. 382. Cold Spring Harbor Laboratory, Cold Spring Harbor, N.Y.
28. **Mothes, W., A. L. Boerger, S. Narayan, J. M. Cunningham, and J. A. Young.** 2000. Retroviral entry mediated by receptor priming and low pH triggering of an envelope glycoprotein. Cell **103:**679–689.
29. **Paquette, Y., Z. Hanna, P. Savard, R. Brousseau, Y. Robitaille, and P. Jolicoeur.** 1989. Retrovirus-induced murine motor neuron disease: mapping the determinant of spongiform degeneration within the envelope gene. Proc. Natl. Acad. Sci. USA **86:**3896–3900.
30. **Perelson, A. S., A. U. Neumann, M. Markowitz, J. M. Leonard, and D. D. Ho.** 1996. HIV-1 dynamics in vivo: virion clearance rate, infected cell life-span, and viral generation time. Science **271:**1582–1586.
31. **Rasty, S., B. R. Dhruva, R. L. Schiltz, D. S. Shih, C. J. Issel, and R. C. Montelaro.** 1990. Proviral DNA integration and transcriptional patterns of equine infectious anemia virus during persistent and cytopathic infections. J. Virol. **64:**86–95.
32. **Resnick-Roguel, N., H. Burstein, J. Hamburger, A. Panet, A. Eldor, I. Vlodavsky, and M. Kotler.** 1989. Cytocidal effect caused by the envelope glycoprotein of a newly isolated avian hemangioma-inducing retrovirus. J. Virol. **63:**4325–4330.
33. **Rice, N. R., A. S. Lequarre, J. W. Casey, S. Lahn, R. M. Stephens, and J. Edwards.** 1989. Viral DNA in horses infected with equine infectious anemia virus. J. Virol. **63:**5194–5200.
34. **Riedel, N., E. A. Hoover, R. E. Dornsife, and J. I. Mullins.** 1988. Pathogenic and host range determinants of the feline aplastic anemia retrovirus. Proc. Natl. Acad. Sci. USA **85:**2758–2762.
35. **Smith, R. E., and E. V. Schmidt.** 1982. Induction of anemia by avian leukosis viruses of five subgroups. Virology **117:**516–518.
36. **Stevenson, M., C. Meier, A. M. Mann, N. Chapman, and A. Wasiak.** 1988. Envelope glycoprotein of HIV induces interference and cytolysis resistance in CD4+ cells: mechanism for persistence in AIDS. Cell **53:**483–496.
37. **Verhoven, B., R. A. Schlegel, and P. Williamson.** 1995. Mechanisms of phosphatidylserine exposure, a phagocyte recognition signal, on apoptotic T lymphocytes. J. Exp. Med. **182:**1597–1601.
38. **Weller, S. K., A. E. Joy, and H. M. Temin.** 1980. Correlation between cell killing and massive second-round superinfection by members of some subgroups of avian leukosis virus. J. Virol. **33:**494–506.
39. **Weller, S. K., and H. M. Temin.** 1981. Cell killing by avian leukosis viruses. J. Virol. **39:**713–721.
40. **Wong, P. K., P. F. Szurek, E. Floyd, K. Saha, and B. R. Brooks.** 1991. Alteration from T- to B-cell tropism reduces thymic atrophy and cytocidal effects in thymocytes but not neurovirulence induced by ts1, a mutant of Moloney murine leukemia virus TB. Proc. Natl. Acad. Sci. USA **88:**8991–8995.
41. **Zingler, K., and J. A. Young.** 1996. Residue Trp-48 of Tva is critical for viral entry but not for high-affinity binding to the SU glycoprotein of subgroup A avian leukosis and sarcoma viruses. J. Virol. **70:**7510–7516.